PAPER

Check for updates

Thickness dependent thermal performance of a poly(3,4-ethylenedioxythiophene) thin film synthesized *via* an electrochemical approach†

Shen Chen,[ab] Tian Luan,[ab] Chen Di,[c] Ming-Hui Lu,[c] Xue-Jun Yan,*[c] Chengyi Song (ID) *[ab] and Tao Deng (ID) [ab]

Polymer-based thermal interface materials (TIMs) have attracted wide attention in the field of thermal management because of their outstanding properties including light weight, low cost, corrosion resistance and easy processing. However, the low thermal conductivity ($\sim$0.2 W m^{-1} K^{-1}) of the intrinsic polymer matrix largely degrades the overall thermal performance of polymer-based TIMs even those containing highly thermal conductive fillers. Hence, enhancing the intrinsic thermal conductivity of the polymer matrix is one of the most critical problems needed to be solved. This paper studies the thermal conductivity of poly(3,4-ethylenedioxythiophene) (PEDOT) films fabricated *via* cyclic voltammetry. By controlling the number of cycles in the electrochemical synthesis, different thickness of PEDOT films could be obtained. A time-domain thermoreflectance (TDTR) system was employed to evaluate the thermal performance of such as-prepared PEDOT films. We have demonstrated that a PEDOT film with thickness of 40 nm achieves the highest out-of-plane thermal conductivity of $\sim$0.60 W m^{-1} K^{-1}, which is almost three folds the thermal conductivity of commercially available pristine PEDOT:PSS film with similar thickness. The X-ray diffraction spectrum reveals that the PEDOT thin film with high crystallinity at the initial stage of electrochemical synthesis leads to enhanced thermal transportation. The findings in this work not only offer an opportunity to fabricate polymer materials exhibiting enhanced thermal conductivity, but also allow one to adjust the thermal performance of conducting polymers in practical applications.

Introduction

Poly(3,4-ethylenedioxythiophene) (PEDOT) and its doped mixtures are some of the most widely studied conducting polymers due to their high electrical conductivity, easy processability and chemical stability.[1–3] Pristine PEDOT films, however, like most polymers, usually possess low thermal conductivity ($\sim$0.2 W m^{-1} K^{-1}),[4] that hinders their practical thermal management applications for organic electronics and batteries, where high thermal conductivity is required.[5] Commercially available PEDOT solutions are composed of PEDOT and surfactant poly(styrenesulfonate) (PEDOT:PSS).[6] This surfactant enables the dispersion of PEDOT molecules in solutions and makes the post-processing techniques easier to perform, enhancing the physical properties of PEDOT films.[7,8] Post-treating PEDOT films with polar solvents (*e.g.* dimethyl sulfoxide (DMSO),[9] ethylene glycol (EG),[10] *etc.*) or acids[11] is a currently traditional and effective strategy to change the thermal conductivity. Liu *et al.* drop-casted DMSO-mixed PEDOT:PSS aqueous solution into films and an out-of-plane thermal conductivity of around 0.3 W m^{-1} K^{-1} was achieved.[9] Hinckley *et al.* deposited the PEDOT:PSS film on a wafer, and then treated it with EtOH solution. Such a post-treated film exhibited a thermal conductivity of around 0.31 W m^{-1} K^{-1} in the out-of-plane direction.[12] Yamaguchi *et al.* mixed commercially-available PEDOT:PSS solution with 5 vol% EG and then spin-casted the mixed solution.[10] After baking, the obtained film with a thickness of 70 nm possessed an out-of-plane thermal conductivity of around 0.29 W m^{-1} K^{-1}.

The reported out-of-plane thermal conductivities of PEDOT and its derivatives are almost no more than 0.3 W m^{-1} K^{-1}.[2,9,10,12–14] Such a low thermal conductivity is as expected due to strong phonon scatterings arising from the disorder in structures, where molecular chains of PEDOT always entangle or twist with each other.[4–6] Even though the existence of rigid and oriented backbone of PSS in PEDOT:PSS facilitates phonon transportation,[15] and can elevate the in-plane thermal

[a] State Key Laboratory of Metal Matrix Composites, School of Materials Science and Engineering, Shanghai Jiao Tong University, 800 Dong Chuan Road, Shanghai 200240, P. R. China. E-mail: chengyi2013@sjtu.edu.cn

[b] Center of Hydrogen Science, Shanghai Jiao Tong University, 800 Dong Chuan Road, Shanghai 200240, P. R. China

[c] College of Engineering and Applied Sciences, Nanjing University, 163 Xianlin Avenue, Qixia District, Nanjing, Jiangsu, 210093, P. R. China. E-mail: xjyan@nju.edu.cn

† Electronic supplementary information (ESI) available. See DOI: 10.1039/d1ra07991c

conductivity over 1.0 W m^{-1} K^{-1}.[9,10,16] The out-of-plane thermal conductivity, which is of critical significance in thermal management applications including thermal interface materials (TIMs), is still around 0.3 W m^{-1} K^{-1}. Spin-coating, drop-casting and some other methods based on solution processing to simply cast polymer into films are not enough to give any control on the microstructures during the formation of polymer films, even followed by post-treatment, the obtained thermal conductivity still remains low. Xu *et al.*[17] has reported that ultradrawn polyethylene films can achieve the thermal conductivity up to 62 W m^{-1} K^{-1}. Zeng *et al.*[18] used electrospinning to produce the fibrous epoxy films with the thermal conductivity as high as 0.8 W m^{-1} K^{-1}. Although stretching[17] and electrospinning[18] have successfully mitigated the structural disorder-induced low thermal conductivity,[19] these methods are not practical for TIMs since they can only deal with the in-plane thermal conductivity leaving out-of-plane thermal conductivity still remaining poor. With respect to the enhancement of out-of-plane thermal conductivity, Smith *et al.*[20] infiltrated regioregular poly(3-hexylthiophene) (rr-P3HT) solution into the nanochannels of anodic aluminium oxide (AAO) templates to orient the arrangement of polymer chains along the nanochannels.

Followed by evaporation and etching of AAO, they obtained P3HT arrays with thermal conductivity up to 1 ± 0.2 W m^{-1} K^{-1}. However, it involves too complicated processing flow to be realized for commercial production.

To overcome the deficiencies of these methods on the thermal conductivity, bottom-up synthesis enabling controllable growth of polymer is under exploration. Oxidative chemical vapor deposition (oCVD) can control the crystallinity and morphology of deposited polymer film by tuning the parameters such as temperature, substrate and oxidative agent.[21–23] Wang *et al.* adopted the oCVD approach to molecularly engineer the crystallization-orientation of PEDOT films by controlling the temperature and film thickness, and then greatly enhanced the electrical conductivity and carrier mobility of the obtained PEDOT films.[24] Smith *et al.* used oCVD to grow 53 nm PEDOT film with thermal conductivity of 0.319 W m^{-1} K^{-1} measured by 3ω method.[25] Though the oCVD approach provides a precise modulation on the molecular-level structure, the complicated equipment and relatively high cost are not affordable in many practical applications. As a traditional method, electropolymerization provides an alternative and easy-to-implement way to achieve bottom-up synthesis of PEDOT by the assembly
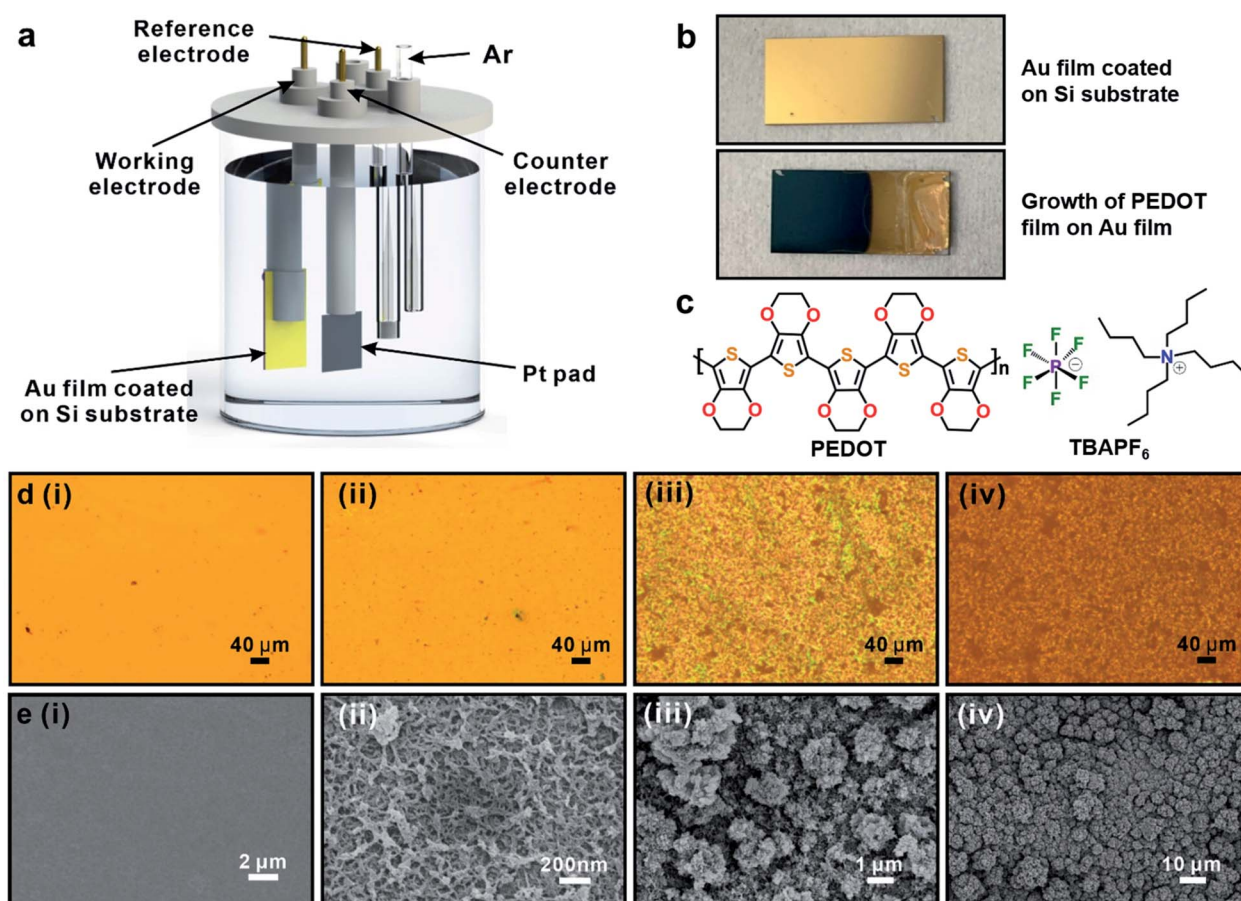
Fig. 1 (a) Schematic of the experimental setup for the electropolymerization of PEDOT; (b) the optical images of as-synthesized PEDOT thin film on the Au-coated silicon substrate; (c) the molecular structures of PEDOT and TBAPF$_6$. (d) Digital photos and (e) scanning electron microscopy (SEM) images of the PEDOT conducting polymer films fabricated by electropolymerization *via* cyclic voltammetry with the cycles of 0 (i), 3 (ii), 10 (iii), 20 (iv).

of EDOT monomers.[26,27] Singh *et al.* electropolymerized arrays of PEDOT nanofibers using AAO templates.[28] The nano-confinement effect induced the oriented growth of molecular chains so that the thermal conductivity of an individual fiber was up to 4.4 W m^{-1} K^{-1}. However, for arrays of PEDOT nanofibers, the thermal conductivity decreased to 0.8–1.0 W m^{-1} K^{-1}. Additionally, removing AAO templates and keeping nanofibers standing without collapsing is not applicable.

In this work, we used template-less electropolymerization instead of high-cost oCVD to synthesize PEDOT films, and studied the thermal performance of PEDOT films. In avoidance of involving complicate treatments after using templates, we directly deposited PEDOT on the Au-coated silicon substrate and studied the variance of thermal conductivity during the growth of PEDOT films. By applying time-domain thermore-flectance (TDTR) to measure the out-of-plane thermal conductivity of films, we observed thickness-dependent thermal conductivity in PEDOT films, where the thermal conductivity of PEDOT film was reduced with the increase of thickness, indicating structural changes during the growth. With the thickness around 40 nm, the out-of-plane thermal conductivity is up to 0.6 W m^{-1} K^{-1}, higher than the bulk thermal conductivity of 0.2 W m^{-1} K^{-1} for most polymers. We analyzed the evolution of morphology and structures in the growth of the PEDOT, and concluded that the degree of structural order is the key factor in the thickness-dependent thermal conductivity. The study on the thermal performance of electropolymerized PEDOT films during the growth gives an exploratory insight in developing electrochemical method as an effective way to modulate the thermal performance of polymer, and the tunable thermal performance shows great prospects in applications such as sensors, thermoelectric devices and thermal management systems.

Results and discussion

Electropolymerization of PEDOT films and their surface morphology

In this work, we used a conventional three-electrode cell for the electropolymerization by an electrochemical workstation (Fig. 1a). A platinum pad served as the counter electrode, and an Ag/Ag$^+$ (0.1 M AgNO$_3$) quasi-reference electrode was home-made and directly immersed in the electrolyte solution. The prepared silicon substrates deposited with a layer of Au acted as the working electrode (Fig. 1b). 3,4-Ethylenedioxythiophene monomers and tetrabutylammonium hexafluorophosphate (TBAPF$_6$) (Fig. 1c) were used for the electropolymerization of PEDOT. Acetonitrile was used as solvent to prepare the electrolyte composed of 0.1 M TBAPF$_6$ and 10 mM EDOT in a 500 ml flask. After slowly pouring the electrolyte into the electrolytic cell, the electrolyte was purged with nitrogen for at least 15 minutes prior to use. Dark blue PEDOT film was then electrochemically synthesized by cyclic voltammetry (Fig. 1b), and meanwhile, the nitrogen was kept purged in avoidance of oxygen. As-synthesized samples were rinsed with acetonitrile and dried in air for subsequent characterizations and tests. Fig. 1d(i) and e(i) show the optical micrograph and scanning

electron microscopy (SEM) image of Au film surface, respectively. Fig. 1d(ii)–(iv) are the optical micrographs of synthesized PEDOT films *via* cyclic voltammetry with the number of cycles 3, 10 and 20, which corresponds to the thickness of 250 nm, 1.84 μm and 11.41 μm measured by profilometer. The color of optical photos changes with the increase of cycle numbers due to the reflection caused by the increasing thickness of PEDOT film. Although the surface texture in Fig. 1d(ii) (3 cycles) behaves almost no difference from pure Au film surface, SEM image (Fig. 1e(ii)) reveals that PEDOT has already grown on the Au film and makes the surface rough. By closely examining Fig. 1e(iii) and (iv), the island structures composed of PEDOT oligomers distribute over the substrate, which facilitate the further growth of PEDOT film and become denser. With the increase of cycle numbers, the thickness and surface roughness of PEDOT film increase gradually.

Thermal conductivity measurement by TDTR system

In this work, we utilized TDTR system to evaluate the thermal conductivity of as-prepared PEDOT films since this method is suitable for measuring thermal conductivity of samples with nanoscale thickness. A schematic diagram of our system is shown in Fig. 2a and the detailed information of TDTR instrument[29–31] is presented in ESI.†

To test the reliability of our TDTR system, we measured the thermal conductivity of silicon substrate. We deposited an aluminium (Al) layer with thickness of 50 nm on the silicon
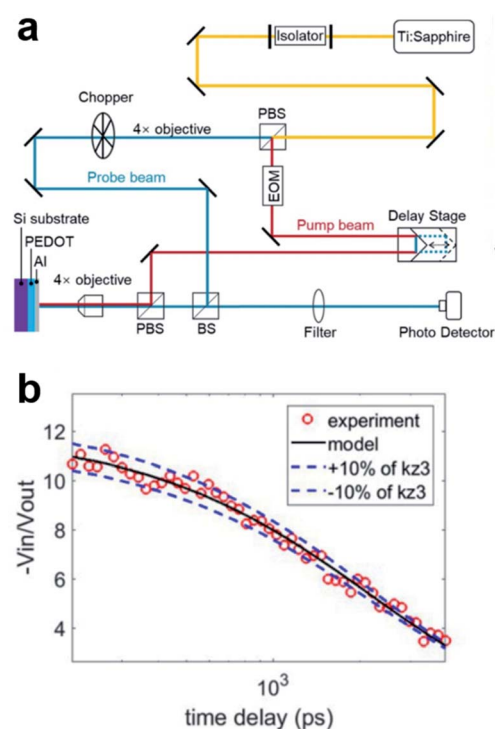
Fig. 2 (a) Schematic illustration of time-domain thermoreflectance (TDTR) system. (b) The ratio of the phase-to-phase voltage under different time delay in the process of the thermal conductivity test for silicon substrate.

RSC Advances

View Article Online

Paper

Open Access Article. Published on 12 January 2022. Downloaded on 2/10/2026 5:38:47 PM. This article is licensed under a Creative Commons Attribution-NonCommercial 3.0 Unported Licence.

substrate, which acts as a transducer layer to monitor the temperature evolution caused by laser heating and heat dissipation in the substrate. Then, we can get the out-of-plane thermal conductivity of silicon substrate by fitting the temperature reduction rate according to multilayer thermal transport model. We have measured several different positions on samples to ensure the repeatability of testing results and the obtained thermal conductivity of Si substrate was 146.42 ± 4.31 W m^{-1} K^{-1}. In reference to the recommended value of 148 W m^{-1} K^{-1} for single crystal silicon at room temperature,[32] the experimental result confirms the reliability of the TDTR system used for the measurement.

Fig. 2b demonstrates the representative raw data with time delays of 0–4 ns in the TDTR measurement. The circular scatter point is the experimental data, and the black solid line is the theoretical fitting curve. There is a relatively good fit between the experiment data and the model with an error tolerance (blue dashed line) within 10%. We also analyzed the sensitivities of silicon coated with Au films in ESI.†

The measurement on the thermal conductivity of electropolymerized PEDOT films

Before the TDTR measurements of electropolymerized PEDOT film, we tested the thickness and surface roughness of the as-prepared PEDOT films. Fig. 3a and b show two-dimensional and three-dimensional AFM images of the surface texture of PEDOT films prepared by cyclic voltammetry (3 cycles). The surface roughness of PEDOT film is $R_a = 17.9$ nm and $R_q = 23.5$ nm, which is larger than that of Au film. However, it still satisfies the requirement for TDTR measurement. Fig. 3c shows the schematic diagram of the multilayer model for PEDOT film coated with Al layer. With the similar measurement process above, we measured the thermal conductivity of PEDOT films with the thickness of ~250 nm. We also analyzed the test sensitivity in the PEDOT film sample, as shown in Fig. S1.† The out-of-plane thermal conductivity of PEDOT film with thickness of ~250 nm is 0.272 W m^{-1} K^{-1}, which is close to the thermal conductivity value of bulk polymer.[19] Previous work have reported that thicker polymer films or fibers tended to produce low thermal or electrical conductivities, which is related to microstructure and crystallization.[18,21,24] Therefore, we reasoned that the low thermal conductivity of PEDOT film with thickness of ~250 nm was due to the disordered microstructures and crystal domains inside PEDOT film. Such disordered structures result in strong phonon scatterings between crystal domains and obstruct thermal transportation. To enhance thermal conductivity of electropolymerized PEDOT film, we decreased the number of cycles during cyclic voltammetry to reduce the thickness of PEDOT film. As shown in Fig. 3d, when the thickness of PEDOT film decreased to ~100 nm (1.5 cycles), the thermal conductivity increased to 0.546 W m^{-1} K^{-1}. On the
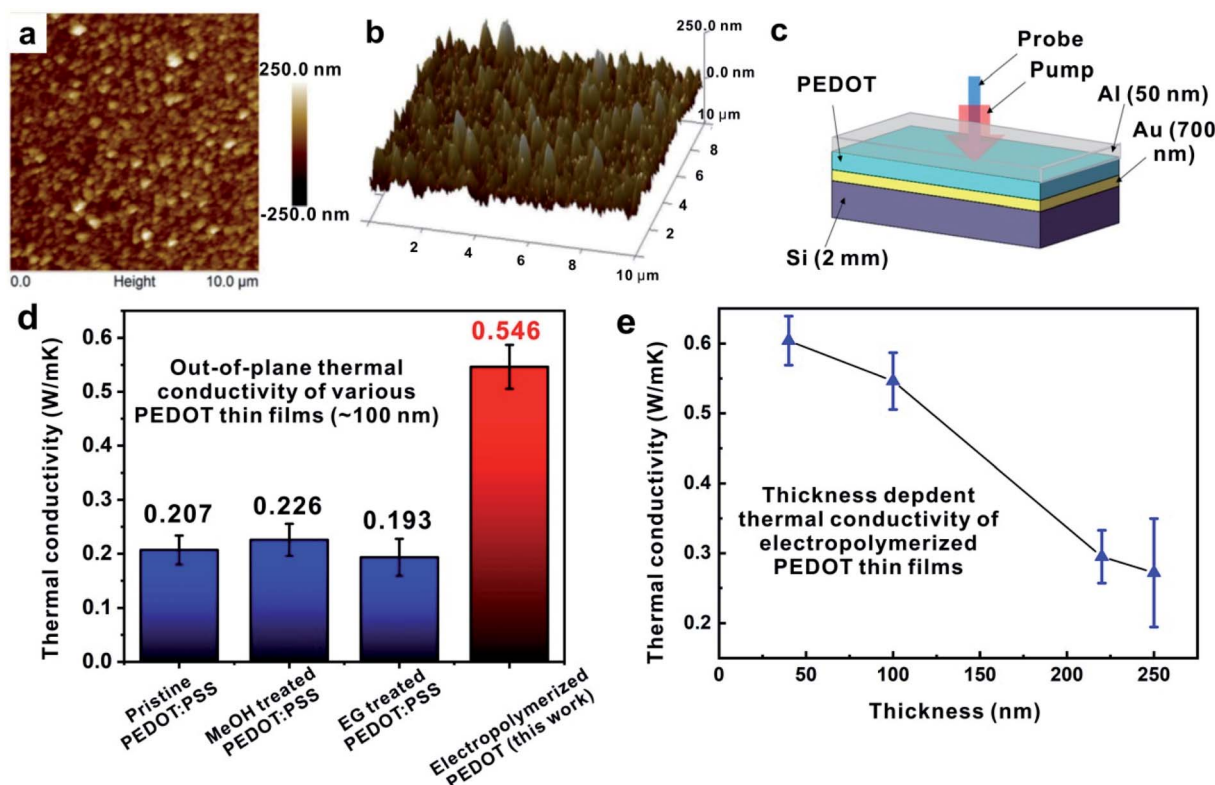

Fig. 3 AFM image of surface roughness for PEDOT film (a) and three-dimensional AFM image of PEDOT film (250 nm) (b). (c) Sample model of PEDOT film coated on Au film for TDTR measurement. (d) Out-of-plane thermal conductivities of commercially available PEDOT:PSS films after various post treatments and PEDOT film fabricated by electropolymerization. (e) The dependence of thermal conductivities on the thickness of PEDOT films fabricated by electropolymerization.

contrary, the out-of-plane thermal conductivity of commercial available PEDOT:PSS film with similar thickness is only 0.207 W m^{-1} K^{-1} (Fig. 3d). Even after applying traditional post-treatments to pristine PEDOT:PSS film, the out-of-plane thermal conductivity still remained lower compared to our electropolymerized PEDOT film. Hence, the thermal conductivity of PEDOT film can indeed be enhanced by electro-polymerization method. To further explore the impact of thickness of electropolymerized PEDOT film on the thermal performance, we have synthesized the PEDOT films with different thickness and measured their thermal conductivities. From Fig. 3e, we observed thickness-dependent thermal conductivity of the PEDOT film, where the thermal conductivity decreases as the film thickness increases. The maximum thermal conductivity is up to 0.604 W m^{-1} K^{-1} when the film thickness is 40 nm (0.5 cycles), indicating that the electro-chemical synthesis method used in this work can significantly improve the out-of-plane thermal conductivity of PEDOT films to a certain extent compared to common methods of solution processing such as drop-casting or spin-coating.[14] Due to the limited reliability of TDTR for samples with thickness less than 40 nm, we did not take a further study on thinner PEDOT films. However, we can speculate from the trend that the thermal conductivity can be further enhanced when the film thickness is below 40 nm. We attributed the thickness-dependent thermal conductivity to the changes in the microstructures of film, where high-order structures exist in thinner films, which will result in a reduced phonon scattering.

Mechanism behind the thickness-dependent thermal conductivity

The doping levels of PEDOT films with different thickness were analyzed by XPS and the results are shown in Fig. S4.† The doping level can be calculated by the atom ratio of sulfur ion (S$^+$) and sulfur (S) in all chemical states (S$_{total}$ = S$_0$ + S$^+$ + S$_{shake-up}$)[33] as shown in Fig. S4(b).† The obtained doping levels are 33%, the same for all PEDOT films with different thickness as illustrated by the overlapped peaks of PEDOT films with different thickness. Such result indicates that the thickness-dependent thermal conductivities obtained were thus not affected by the doping levels since all the doping levels are the same. Besides, PEDOT is well-known for its best atmospheric stability among conducting polymers.[34–36] Therefore, the stability of the PEDOT film with the doping level of 33% was tested by keeping the PEDOT film in air for 8 days. The result given by XPS showed that the doping level maintained around 33% (Fig. S5†), the same as that of the original sample, which demonstrated the stability of the PEDOT. Fig. 4a shows the X-ray diffraction spectrum of PEDOT films of different thickness fabricated by cyclic voltammetry. In the electrochemically synthetic process, we controlled the number of cycles, and kept the standing potential and the scan rate constant, from −0.2 V to 0.9 V at 100 mV s^{-1}. The diffraction peak in Fig. 4a can be assigned to (200) at 2θ of 13.0°, as is similar to previous XRD pattern of PEDOT films doped with TBAPF$_6$.[37] Obviously, the peak corresponding to (200) of the 40 nm film is the sharpest and the peak
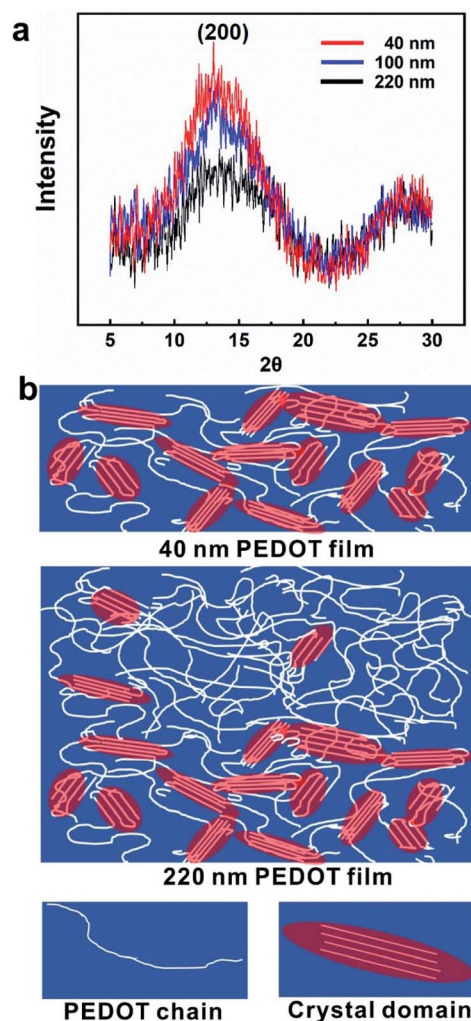

Fig. 4 (a) XRD results for the PEDOT films with different thickness; (b) schematic of the distribution of crystalline regions within PEDOT thin films at different growth stages (different thickness).

of the 100 nm film is close to that peak, while the 220 nm film (2.5 cycles) shows least sharp peak. The peak pattern of XRD analysis indicates the progress of structural evolution during the growth of PEDOT films and the different structure in films with different thickness. According to previous work, two groups of four PEDOT chains partly stacking in the direction perpendicular to the molecular plane side by side form the crystal unit cell in electropolymerized PEDOT films.[37,38] The crystallinity of the whole film depends on the number of such crystalline units. The regular structure within crystalline greatly reduces phonon scatterings and provides highway for phonons transportation, hence enhances the thermal conductivity compared to other amorphous area, where disordered molecular chains including distortion and entanglement heavily hinder the effective phonon transportation.[4,17] A broadened peak for the 220 nm film indicates a lower degree of crystallinity, implying the lack of structural order. In contrast, a higher degree of crystallinity in the 40 nm film produces high density of ordered crystalline zones, which lead to a higher thermal

conductivity. Based on the experimental results, we hypothesized the mechanism of thickness-dependent thermal conductivity of electropolymerized PEDOT film and the schematic is shown in Fig. 4b. At the initial stage, during the growth of polymer film, polymer molecular chains are short and not easy to twist and entangle, resulting in thin films with more crystalline zones and smooth film surface. With the growth proceeding, molecular chains grow longer and tend to become disordered.[21] The surface becomes rougher and the crystallinity is reduced, which is consistent with the results of surface roughness and XRD of PEDOT films with different thicknesses. Therefore, the thermal conductivity measured in this work shows a downward trend with the increase of thickness of PEDOT film in the sample.

Conclusions

In summary, we have prepared PEDOT films with different thickness *via* cyclic voltammetry, studied thickness-dependent thermal conductivity of as-prepared PEDOT film, and discussed mechanistic insight of thermal transport capability relying on the inner structures of PEDOT film. TDTR measurement reveals that, with the increase of thickness of as-prepared PEDOT film, its out-of-plane thermal conductivity shows a downward trend, which is related to the decrease of crystallinity and disorder degree of molecular chains inside polymer film. In our work, 40 nm as-prepared PEDOT film exhibits the highest thermal conductivity of $0.60 \text{ W m}^{-1} \text{ K}^{-1}$, which is about 100% higher than that of post-treated PEDOT:PSS film reported previously. It indicates that the electrochemical synthesis method used in this study can not only improve the out-of-plane thermal conductivity of PEDOT films, but also allow one to tune the thermal performance of electropolymerized PEDOT film by simply adjusting electrochemical synthetic conditions.

Conflicts of interest

There are no conflicts to declare.

Acknowledgements

References

1 T. P. Kaloni, P. K. Giesbrecht, G. Schreckenbach and M. S. Freund, *Chem. Mater.*, 2017, **29**, 10248–10283.

2 Y. Xu, Y. Jia, P. Liu, Q. Jiang, D. Hu and Y. Ma, *Chem. Eng. J.*, 2021, **404**, 126552.

3 Y. Yang, H. Deng and Q. Fu, *Mater. Chem. Front.*, 2020, **4**, 3130–3152.

4 N. Mehra, L. Mu, T. Ji, X. Yang, J. Kong, J. Gu and J. Zhu, *Appl. Mater. Today*, 2018, **12**, 92–130.

5 X. Xu, J. Chen, J. Zhou and B. Li, *Adv. Mater.*, 2018, **30**, e1705544.

6 S. M. Kim, C. H. Kim, Y. Kim, N. Kim, W. J. Lee, E. H. Lee, D. Kim, S. Park, K. Lee, J. Rivnay and M. H. Yoon, *Nat. Commun.*, 2018, **9**, 3858.

7 B. Friedel, P. E. Keivanidis, T. J. K. Brenner, A. Abrusci, C. R. McNeill, R. H. Friend and N. C. Greenham, *Macromolecules*, 2009, **42**, 6741–6747.

8 J. Luo, D. Billep, T. Waechtler, T. Otto, M. Toader, O. Gordan, E. Sheremet, J. Martin, M. Hietschold, D. R. T. Zahn and T. Gessner, *J. Mater. Chem. A*, 2013, **1**, 7576–7583.

9 J. Liu, X. Wang, D. Li, N. E. Coates, R. A. Segalman and D. G. Cahill, *Macromolecules*, 2015, **48**, 585–591.

10 S. Yamaguchi, T. Shiga, S. Ishioka, T. Saito, T. Kodama and J. Shiomi, *Rev. Sci. Instrum.*, 2021, **92**, 034902.

11 Z. Fan, P. Li, D. Du and J. Ouyang, *Adv. Energy Mater.*, 2017, **7**, 1602116.

12 A. C. Hinckley, S. C. Andrews, M. T. Dunham, A. Sood, M. T. Barako, S. Schneider, M. F. Toney, K. E. Goodson and Z. Bao, *Adv. Electron. Mater.*, 2021, **7**, 2001190.

13 Z. Fan and J. Ouyang, *Adv. Electron. Mater.*, 2019, **5**, 1800769.

14 Y. Zheng, H. Zeng, Q. Zhu and J. Xu, *J. Mater. Chem. C*, 2018, **6**, 8858–8873.

15 Q. Wei, M. Mukaida, K. Kirihara and T. Ishida, *ACS Macro Lett.*, 2014, **3**, 948–952.

16 A. Weathers, Z. U. Khan, R. Brooke, D. Evans, M. T. Pettes, J. W. Andreasen, X. Crispin and L. Shi, *Adv. Mater.*, 2015, **27**, 2101–2106.

17 Y. Xu, D. Kraemer, B. Song, Z. Jiang, J. Zhou, J. Loomis, J. Wang, M. Li, H. Ghasemi, X. Huang, X. Li and G. Chen, *Nat. Commun.*, 2019, **10**, 1771.

18 X. Zeng, L. Ye, K. Guo, R. Sun, J. Xu and C.-P. Wong, *Adv. Electron. Mater.*, 2016, **2**, 1500485.

19 C. Huang, X. Qian and R. Yang, *Mater. Sci. Eng., R*, 2018, **132**, 1–22.

20 M. K. Smith, V. Singh, K. Kalaitzidou and B. A. Cola, *ACS Nano*, 2015, **9**, 1080–1088.

21 S. P. Arnold, J. K. Harris, B. Neelamraju, M. Rudolph and E. L. Ratcliff, *Synth. Met.*, 2019, **253**, 26–33.

22 K. K. Gleason, *Nat. Rev. Phys.*, 2020, **2**, 347–364.

23 K. K. Gleason, *J. Vac. Sci. Technol., A*, 2020, **38**, 020801.

24 X. Wang, X. Zhang, L. Sun, D. Lee, S. Lee, M. Wang, J. Zhao, Y. Shao-Horn, M. Dincă, T. Palacios and K. K. Gleason, *Sci. Adv.*, 2018, **4**, eaat5780.

25 P. M. Smith, L. Su, W. Gong, N. Nakamura, B. Reeja-Jayan and S. Shen, *RSC Adv.*, 2018, **8**, 19348–19352.

26 L. Groenendaal, G. Zotti, P. H. Aubert, S. M. Waybright and J. R. Reynolds, *Adv. Mater.*, 2003, **15**, 855–879.

27 M. J. Donahue, A. Sanchez-Sanchez, S. Inal, J. Qu, R. M. Owens, D. Mecerreyes, G. G. Malliaras and D. C. Martin, *Mater. Sci. Eng., R*, 2020, **140**, 100546.

28 V. Singh, T. L. Bougher, A. Weathers, Y. Cai, K. Bi, M. T. Pettes, S. A. McMenamin, W. Lv, D. P. Resler,

T. R. Gattuso, D. H. Altman, K. H. Sandhage, L. Shi, A. Henry and B. A. Cola, *Nat. Nanotechnol.*, 2014, **9**, 384–390.

29 C. Di, J.-H. Pan, S.-T. Dong, Y.-Y. Lv, X.-J. Yan, J. Zhou, S.-H. Yao, H. Lu, V. E. Gusev, Y.-F. Chen and M.-H. Lu, *CrystEngComm*, 2019, **21**, 6261–6268.

30 X.-J. Yan, Y.-Y. Lv, L. Li, X. Li, S.-H. Yao, Y.-B. Chen, X.-P. Liu, H. Lu, M.-H. Lu and Y.-F. Chen, *Appl. Phys. Lett.*, 2017, **110**, 211904.

31 L. Cao, J. Pan, H. Zhang, Y. Zhang, Y. Wu, Y.-Y. Lv, X.-j. Yan, J. Zhou, Y. B. Chen, S.-h. Yao, Y. Pei, M.-h. Lu and Y.-f. Chen, *J. Phys. Chem. C*, 2019, **123**, 27666–27671.

32 Y. Ma, *J. Appl. Phys.*, 2014, **116**, 243505.

33 A. Et Taouil, F. Lallemand, J. Y. Hihn, J. M. Melot, V. Blondeau-Patissier and B. Lakard, *Ultrason. Sonochem.*, 2011, **18**, 140–148.

34 S. Kirchmeyer and K. Reuter, *J. Mater. Chem.*, 2005, **15**, 2077–2088.

35 Q. Wei, M. Mukaida, K. Kirihara, Y. Naitoh and T. Ishida, *Materials*, 2015, **8**, 732–750.

36 M. Łapkowski and A. Proń, *Synth. Met.*, 2000, **110**, 79–83.

37 L. Niu, C. Kvarnström, K. Fröberg and A. Ivaska, *Synth. Met.*, 2001, **122**, 425–429.

38 K. E. Aasmundtveit, E. J. Samuelsen, L. A. A. Pettersson, O. Inganäs, T. Johansson and R. Feidenhans'l, *Synth. Met.*, 1999, **101**, 561–564.